http://dx.doi.org/10.5935/0103-5053.20150322

J. Braz. Chem. Soc., Vol. 27, No. 4, 727-734, 2016.
Printed in Brazil - ©2016 Sociedade Brasileira de Química
0103 - 5053 $6.00+0.00

Article

Hybrid Self-Assembled Materials Constituted by Ferromagnetic Nanoparticles and Tannic Acid: a Theoretical and Experimental Investigation

Anderson F. M. Santos,[a] Lucyano J. A. Macedo,[a] Mariana H. Chaves,[a] Marisol Espinoza-Castañeda,[b] Arben Merkoçi,[b] Francisco das Chagas A. Lima[c] and Welter Cantanhêde*[,a]

[a]*Departamento de Química, Universidade Federal do Piauí, 64049-550 Teresina-PI, Brazil*

[b]*Institut Català de Nanociencia i Nanotecnologia (ICN2) & ICREA, Universitat Autònoma de Barcelona, Campus Bellaterra, 08193 Barcelona, Spain*

[c]*Centro de Ciências da Natureza, Universidade Estadual do Piauí, 64002-150 Teresina-PI, Brazil*

Hybrid magnetite materials are interesting for both biomedical and catalytic applications due to their well-known biocompatibility, as well as their magnetic and electric properties. In this work we prepared Fe_3O_4 nanoparticles (NPs) coated with tannic acid (TA), a natural polyphenol, through two different synthetic routes, aiming to understand the influence of TA in the synthesis step and contribute to the development of water-dispersible magnetic materials. The coating process was verified by information obtained from transmission electron microscopy (TEM), zeta-potential and Fourier transform infrared (FTIR) spectroscopy. The incorporation of TA after Fe_3O_4 NPs production generated spherical NPs smaller than 10 nm, suggesting that TA plays a fundamental role in the nucleation and organization of Fe_3O_4 NPs. Data from both density functional theory (DFT) and FTIR allowed us to infer that Fe_3O_4 interacts mainly with the carbonyl groups of TA. Hybrid materials having improved water-dispersibility are very attractive for biomedical applications.

Keywords: hybrid materials, magnetite, tannic acid, supramolecular, DFT

Introduction

Hybrid materials (HMs) have attracted special attention over the past two decades as a result of the emergence of novel physicochemical characterization methods. The HM class has opened many perspectives in nanoscience and nanotechology due to the possibility of achieving enhanced properties or specific advanced functional materials.[1] HMs are formed from at least two components that interact on a molecular level, such as metallic nanoparticles, biopolymers, synthetic polymers and inorganic complexes.[2-4] Usually, the interactions between components within HMs come from dynamic covalent (e.g., imine and disulfide bonding) and/or reversible non-covalent interactions (e.g., van der Waals and H-bonding).[5] The formation of hybrid materials can be suitably achieved through self-assembly, since the interactions between components are governed by recognition and self-organization processes at the molecular level.[3,4]

*e-mail: welter@ufpi.edu.br

In order to contribute to the development of water-dispersible magnetic hybrid materials of interest for biomedical applications we explored ferromagnetic nanoparticles (Fe_3O_4 NPs) because of their magnetic and electric properties, biological compatibility, low toxicity[6] and relatively easy preparation. They also have been used in several applications that include magnetic resonance imaging contrast agents,[7] magnetic fluid hyperthermia,[8] media for targeted drug delivery and the magnetic separation of cells.[9] These nanoparticles show novel properties that are different from those of the bulk materials because their small size changes their coordination, symmetry and electronic confinement.[10] These singular properties of Fe_3O_4 NPs are conditioned by the presence of isolated particles because, when together, they tend to aggregate due to strong magnetic dipole-dipole interactions between particles.[11] Aggregation phenomena of the Fe_3O_4 NPs can significantly decrease their interfacial area resulting in the loss of magnetism and dispersibility.[12]

To improve dispersion, these nanoparticles are usually covered by stabilizing agents such as surfactants, polymers,

oxides, metal coating or other natural compounds with some specific functional groups that have been used to modify these particles to increase their stability.[13] Tannic acid (TA), a polyhydric phenolic compound, works as a natural species capable of acting as stabilizer matrix and can make Fe_3O_4 NPs more biocompatible and increase water-dispersibility. TA is a mixed gallotannin composed of hydrolysable polyphenols of high molecular weight, including esters of gallic acid and glucose.[14] TA can be found in the bark of oak, hemlock, chestnut, and in the galls of certain plants.

There are several reported ways to synthesize iron-oxide nanoparticles with diameter sizes ranging from 10 to 100 nm including solvothermal,[15] hydrothermal,[16] sonochemical,[17] microwave[16,18] and co-precipitation[19] methods. We used co-precipitation for the chemical modification of magnetite nanoparticles because of its simplicity and cost effectiveness. It is important to note that several reaction conditions such as temperature, pH, changing the iron salt, rate of addition, and preparation methods alter the type of oxides particles obtained (e.g., size, shape, and mineralogy), which requires special attention during the synthesis procedure.[15-19]

Herrera-Becerra *et al.*[20,21] reported works focusing the biosynthesis of iron oxide nanoparticles ($Fe_{0.902}O$ and Fe_3O_4) using a green chemistry approach. For this purpose, TA was used as modifier and reducer in order to produce metallic particles smaller than 5 nm. Omoike[22] also investigated the preparation of Fe_3O_4 nanoparticles containing TA through co-precipitation and post-precipitation methods. The magnetic nanoparticles synthesized by post-precipitation exhibited higher binding capability for Cu^{II} ions in the presence of Zn^{II} ions than nanoparticles synthesized by co-precipitation method.

In this work, the synthesis strategy reported aims to develop water-dispersible magnetic Fe_3O_4 NPs using TA as a modifier. In addition, we characterize and investigate possible interactions between Fe_3O_4 and TA at the supramolecular level. For this purpose, we used several techniques, including microscopic and spectroscopic methods, X-ray diffraction (XRD), zeta potential, and density functional theory (DFT) calculations.

Experimental

Reagents and materials

$FeCl_2{\cdot}4H_2O$, $FeCl_3{\cdot}6H_2O$ and tannic acid were commercial products purchased from Sigma-Aldrich, while NaOH, KH_2PO_4, and K_2HPO_4 were purchased from Reagen (analytical grade and used with no further purification). All solutions were prepared with ultrapure water, purified by Elga Purelab Option-Q system, with resistivity larger than 18.2 MΩ cm.

Preparation of bare Fe_3O_4 NPs

For control purposes, bare Fe_3O_4 NPs were prepared using a modified version of conventional co-precipitation method.[2] Initially a solution of 50 mL from the precursor salts, $FeCl_2{\cdot}4H_2O$ (100 mg, 5.0×10^{-3} mol) and $FeCl_3{\cdot}6H_2O$ (67.5 mg, 2.5×10^{-4} mol), was prepared in concentrations of 0.01 and 0.005 mol L^{-1}, respectively. This mixture was transferred to a reaction flask and left for 5 minutes under a nitrogen flow. After this step, the 1.0 mol L^{-1} NaOH solution was dripped onto the mixture in an ultrasonic bath (UNIQUE, USC-750A) until the supernatant became translucent, indicating the end of precipitation. The flask containing the product was left for 30 min under heating and ultrasonic bath at 40 °C, in order to enhance the ripening process of the NPs. The washing procedure of the Fe_3O_4 NPs was then performed with a 50% (v/v) water-ethanol solution, separating the precipitate from the supernatant with a magnet, repeating this step until the pH become neutral. The Fe_3O_4 powder was dried in an oven at 100 °C for 15 min.

Preparation of hybrid ferromagnetic materials

The synthesis of hybrid ferromagnetic materials was similar to the synthesis described previously for the bare Fe_3O_4 NPs, with only one change, the addition of 7.5 mL of 0.01 mol L^{-1} TA (170 mg, 1.0×10^{-4} mol) into the system. For production of the TA-Fe_3O_4, TA was added to the solution of Fe^{III}/Fe^{II} before the precipitation of iron oxide. For the production of Fe_3O_4-TA, TA was only added to the solution after the total precipitation of iron oxide by NaOH. For the two hybrid materials, the procedure after the addition of TA was rigorously the same as that used for the Fe_3O_4 NPs production.

Characterization

The infrared spectra of the Fe_3O_4, TA-Fe_3O_4 and Fe_3O_4-TA NPs and TA samples were prepared as KBr pellets and measured in a PerkinElmer FTIR spectrum 100 at the range of 4000-400 cm^{-1}. TEM was performed using a JEOL JEM 2011, operating at an accelerating voltage of 200 kV. A drop of each solution of TA-Fe_3O_4, Fe_3O_4-TA and Fe_3O_4 NPs was cast on the copper grid, dried, and analyzed. XRD analyses were performed on a Shimadzu XRD 600 diffractometer using Cu-K_α radiation with a scan

rate of 2º min^{-1}, and the data (2θ) were collected from 10º to 75º under a continuous scan mode. The zeta potential measurements were carried out in a Malvern Zetasizer Nano-ZS (Malvern Instruments Ltd.) according to the manufacturer's recommendations.

Computational methods

The computational optimization was performed in density functional theory DFT/B3LYP[23-25] combining the 6-31+G** basis set[26] for all atoms and Lanl2DZ[27-29] for iron, using the software Gaussian 09.[30] Fe_3O_4 has a cubic inverse spinel structure where the oxygen anions form a close-packed fcc sublattice with Fe^{II} and Fe^{III} cations located in the interstitial sites.[31] The equal amount of Fe^{II} and Fe^{III} ions occupies the octahedral coordination of oxygen atoms and Fe^{III} ions occupy the tetrahedral coordination of oxygen. In these calculations, the cubic magnetite unit cell was described by a cluster model consisting of 32 atoms ($Fe_{16}O_{16}$) in vacuum to investigate the interaction of TA and (111) Fe_3O_4 surface. It was used the Fd3m space group and the crystal was frozen with the length of cubic cell edge (*a*) equal to 8.394 Å (with R = 90°). Single point calculation was performed to obtain the dipole moment of Fe_3O_4 structure from the cited unit cell.[30]

The binding energy of the TA-Fe_3O_4 system was taken to be the energy difference (ΔE) defined as $\Delta E = E(TA\text{-}Fe_3O_4) - E(TA + Fe_3O_4)$, where the first term is the total energy of the system (TA-Fe_3O_4) and the second term is the energy of the TA and Fe_3O_4, respectively. Only the relaxations of the nearest neighbors to the adsorption site were included in the calculation.

Results and Discussion

Strategy for producing of hybrid tannic acid coated Fe_3O_4 NPs

Aiming to investigate the influence of phenolic compounds on the final physical and chemical properties of the ferromagnetic nanoparticles, we prepared two hybrid materials, here abbreviated as TA-Fe_3O_4 NPs and Fe_3O_4-TA NPs, which were basically differentiated by the incorporation of TA during the synthesis step. As described in the experimental section, TA-Fe_3O_4 is generated by adding TA into the Fe^{II} and Fe^{III} precursor solution, followed by precipitation of the Fe_3O_4 NPs by dropping sodium hydroxide solution. However, the addition of TA to a suspension containing previously formed Fe_3O_4 NPs leads to the formation of Fe_3O_4-TA NPs. This strategy can infer the role of phenolic compounds in the nucleation process of NPs and, consequently, their physical and chemical properties. Additionally, bare Fe_3O_4 NPs (without TA) were used as the experimental control.

After the production of the TA-Fe_3O_4 and Fe_3O_4-TA systems, some simple tests were performed to verify the success of the synthetic routes, such as the magnetism of the materials and observation of the color of the precipitates. Immediately after the preparation, it was possible to visualize that the samples were black and exhibited magnetic attraction when placing a magnet near the reaction flask, as observed in Figure S1 of the Supplementary Information. Since tannic acid functionalized Fe_3O_4 nanoparticles were washed several times after preparation process, the phenolic compound was not dissociated from NPs. The color presented by the dispersion is dependent on the time that the system was exposed to the magnetic field. Nanoparticles were redispersed by sonication.

Spectroscopic characterization and investigation of Fe_3O_4 formation

The UV-Vis spectra for the precursor and hybrid materials are illustrated in Figure 1. Tannic acid exhibited two absorption peaks at 212 and 277 nm, attributed to π→π* and n→π* transitions from aromatic units and C=O groups, respectively.[32] The electronic spectrum from the TA-Fe^{III}/Fe^{II} mixture (Figure 1, inset) showed a broad peak absorption centered at 560 nm, indicating the formation of a chelate complex between Fe^{III} and Fe^{II} ions and TA ligands[33] (equation 1). Bare Fe_3O_4 NPs and hybrid material exhibited a typical broad absorption band in the UV-Vis region,[34] with a contribution of the baseline increasing as a result of the light scattering effects noticeable in colloidal suspension.[35,36]

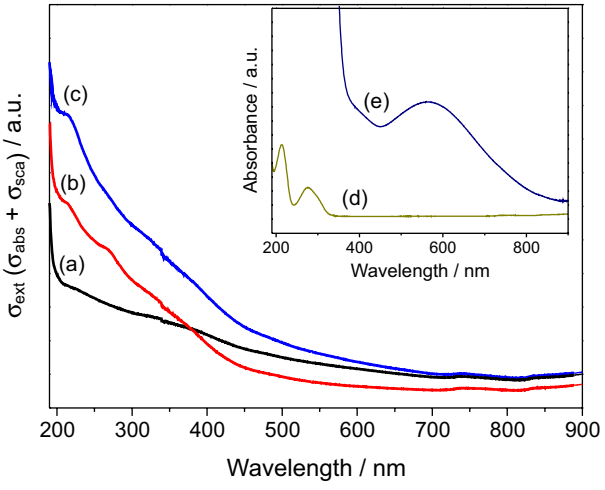

Figure 1. Electronic spectra for (a) Fe_3O_4 NPs; (b) Fe_3O_4-TA and (c) TA-Fe_3O_4. In the inset (d) TA compound and (e) TA-FeI^{III}/Fe^{II} complex.

Both TA-Fe_3O_4 and Fe_3O_4-TA systems showed similar UV-Vis profiles of Fe_3O_4 NPs, and two absorption bands in the UV regions, at 212 and 265 nm, assigned to the TA transitions. It is appropriate to notice that these bands are characteristics of the TA compound. The band centered at 265 nm is blue shifted probably caused by the deformation of TA molecule symmetry as an effect of the supramolecular interaction within the hybrid material. Indeed, the appearance of these characteristic peaks of TA in the electronic spectrum of the hybrid material is related to the fact that TA has been added to the systems, without any interference in the synthesis of the NPs. Similar to the observed in the FTIR investigation, the supramolecular interactions between the compounds through the Fe^{III} (Fe_3O_4) and carbonyl (TA) groups caused a blue-shift of TA species for both hybrid materials (277 to 265 nm).

According to Jaen *et al.*,[37] the conversion reaction of metallic iron to the tannate complex is governed by first-order reaction kinetics with a rate constant of $k = 6.51 \times 10^{-2}$ d^{-1} and estimated time of about 2.3 months (alkaline media, T = 25 ºC). As cited previously, the process of nanoparticle formation is influenced by the NaOH concentration and, in the specific case of the TA-Fe_3O_4, must be guided by the following mechanism, due to the initial complexation step:

$$nTA + Fe^{II} + Fe^{III} \rightleftharpoons n[(TA)_2Fe^{II}\text{-}TA\text{-}Fe^{III}(TA)_2]^{5+} \quad (1)$$

$$n[(TA)_2Fe^{II}\text{-}TA\text{-}Fe^{III}(TA)_2]^{5+} + xOH^- \rightarrow TA_n\text{-}Fe_3O_4 + \frac{x}{2}H_2O \quad (2)$$

Related to this, while comparing the electronic spectrum of the TA-Fe^{III}/Fe^{II} association with the electronic spectra of hybrid materials, we observed a complete disappearance of the band centered at 560 nm, and the presence of one discrete band at 212 nm, leading us to believe that the kinetic process chelating iron cations with TA is disadvantageous, and there is a displacement of the equilibrium to the effective formation of ferromagnetic nanoparticles.

The FTIR spectra of the Fe_3O_4, TA compound, TA-Fe_3O_4 and Fe_3O_4-TA systems are shown in Figure 2. The main bands of the TA compound are 3450 cm^{-1} (O–H stretching, strong), 1740 cm^{-1} (C=O stretching, strong), 1630 cm^{-1} (aromatic C=C stretching, medium), 1198 cm^{-1} (phenolic C–O stretching, medium) and 1088 cm^{-1} (sugar moiety C–O(H) stretching, medium).[38] For the bare Fe_3O_4, the FTIR spectrum shows the main bands at 3450, 1680 and 575 cm^{-1} assigned to O–H stretching, O–H bending, and Fe–O stretching, respectively.[39] The maximum absorption centered at 3420 cm^{-1} for the TA and TA-derivatives is caused by the OH groups, indicating the presence of polyphenols in the materials. Additionally, the band at 1088 cm^{-1} attributed to the stretching vibration of the sugar moiety or CH_2OH groups is shifted to 1066 and 1058 cm^{-1} in the TA-Fe_3O_4 and Fe_3O_4-TA, respectively, and probably associated with the Fe_3O_4 interaction. Another important observation is that after TA is added to the Fe_3O_4 NPs, the absorption related to the C=O stretching of the polyphenol clearly shifts to shorter wavenumbers, and is overlapped in both Fe_3O_4 systems. Furthermore, the Fe_3O_4 spectrum exhibited a typical band at 575 cm^{-1} (medium intensity) related to the stretching mode of the Fe–O bond, which shifts to shorter wavenumbers (565 and 570 cm^{-1}) after the addition of TA in TA-Fe_3O_4 and Fe_3O_4-TA, respectively. Based on these results, we suggest that Fe_3O_4 NPs were successfully coated with TA compound. Results suggest interactions between the negatively charged surface of the Fe_3O_4 and TA are mainly with the C=O groups of polyphenol and in a minor contribution of the aromatic rings and the phenolic hydroxyl groups present in large quantities *per* molecule (as proposed by TEM investigation and zeta potential data). In order to have a better understanding of how the interactions between the TA molecules and iron oxide occur, we performed a computational investigation using DFT theory.

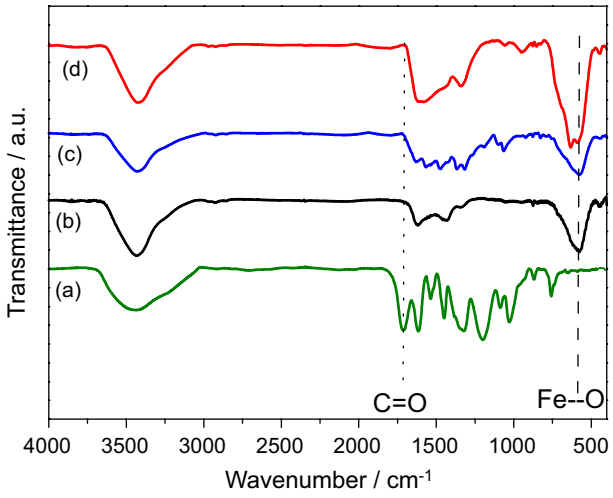

Figure 2. FTIR spectra for (a) TA; (b) Fe_3O_4; (c) TA-Fe_3O_4 and (d) Fe_3O_4-TA in KBr pellets.

Figure 3 shows the optimized structures of two different possibilities for the supramolecular interaction of complex Fe_3O_4 with TA using DFT calculations. The simulation was performed using a cubic unit cell of Fe_3O_4, which was observed as the bond length of Fe–O and Fe=O at 1.960 and 1.680 Å, respectively, and valence angle of Fe–O–Fe equal to 87º. For the bond angle O–Fe=O, this value is 180º. According to Maharramov *et al.*,[40] the dipole momentum values for the optimized structures (using the PM3 method)

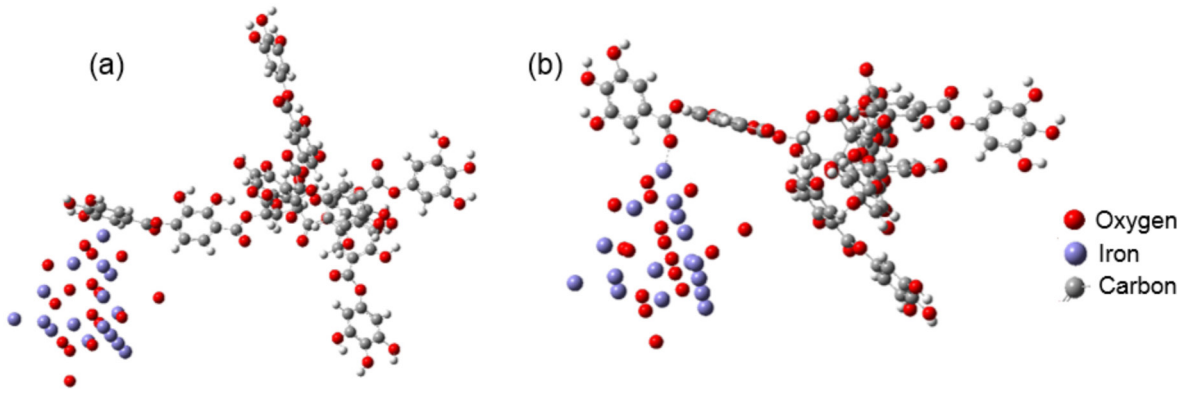

Figure 3. Optimized structures of: (a) interaction between aromatic rings and Fe_3O_4 and (b) interaction between carbonyl groups and Fe_3O_4.

of FeO, Fe_2O_3, and Fe_3O_4 were found to be equal to 1.61, 0.93, and 2.63 D, respectively, indicating that Fe_3O_4 employs a higher character of the molecular interaction with the medium because of its polarity. In this work the dipole momentum calculated for Fe_3O_4 structure was of 2.46 D, which is in agreement with values obtained in the literature.[39] In addition, TA compound showed a distorted structure with bond angle O=C–O calculated at 123.4º. However, the dihedral angle $C_{(CO)}$–O–C_{Ar}–C_{Ar} observed is 170.1º.

This latter value shows that the aromatic rings are out of the plane, producing a distortion of 10º throughout the optimized structure. The bond length calculated for the carbonyl groups (C=O) and groups of polyphenol (C–O) were 1.220 and 1.360 Å, respectively. However, in the TA-Fe_3O_4 complex, these parameters show little change with a variation of 0.007 Å (C=O) and 0.016 Å for the (C–O) groups. The theoretical calculation showed that the relative stabilization energy of the TA-Fe_3O_4 complex, interacting via carbonyl groups (Figure 3b), is 250 kJ mol^{-1} more stable than that observed for TA-complex interacting via the aromatic rings. The binding energy calculated for the most stable complex was estimated to be 420 kJ mol^{-1}, while for the less stable system the calculated energy was 190 kJ mol^{-1}. From these results, we can suggest that the main site of interaction with the nanoparticles occurs through carbonyl groups, converging to the same information provided by FTIR. However, as observed through FTIR spectra, hydroxyl and aromatic rings also contributed in a minor way to bind the TA stabilizer to the Fe_3O_4 NPs. DFT study has been also used to investigate reaction mechanism and gas adsorption study involved on the surface of Fe_3O_4 crystals.[31] For example, Huang *et al.*[31] investigated CO adsorption on Fe_3O_4 surface at different conditions with interest in the catalysis area. In another work, Yang *et al.*[41] used a DFT study to elucidate the reaction mechanism for polyaniline/Fe_3O_4 nanoparticle composite formation.

Molecular structures of hybrid systems constituted by Fe_3O_4 nanoparticles and polyphenol tannic acid

Based on the zeta potential measurements, the surface charges and stabilities of the TA-Fe_3O_4, Fe_3O_4-TA and Fe_3O_4 colloidal suspensions were explored. Since the pH value 14 of the colloidal suspensions of hybrid materials was higher than the pK_a value ca. 10.0 of the TA,[14,22] the gallic acid units that form TA are partially ionized in the hydroxyl *para*-carbonyl position because its conjugate base is better stabilized by resonance than hydroxyl *meta*-carbonyl position. Therefore, there is an unbalance of charge on Fe_3O_4 NPs surfaces (containing TA) probably due to effect of electronic delocalization from the terminal groups.

Negative values for colloidal suspensions of magnetic nanoparticles indicate that the surface of the magnetic nanoparticles produced is negatively charged, thus presenting a prominent anionic character. The zeta potential measurements also indicated that the addition of TA intensifies this nature for both hybrid materials. It is remarkable to note the impact of the TA addition on the zeta potential values of the magnetic nanoparticles. In particular, it was observed that the strongest change on the zeta potential of the materials happened when TA was added before precipitation of the nanoparticles (TA-Fe_3O_4), which presented the most negatively charged surface after nanoparticle formation (Table 1). The increase in the zeta potential value can be explained since the interaction between the TA and Fe_3O_4 nanoparticles occurs via polyphenolic carbonyl groups, it turns the phenolic hydroxyls groups toward the outer, which is evidenced by FTIR and the computational simulation data. In this process, the negative charge from the deprotonated phenolic hydroxyls on the nanoparticles increases the amount of charge on its surface, and thus, increases the zeta potential of the nanoparticles surface.

The increase in the zeta potential values explains why the nanoparticles were not agglomerated and did not

Table 1. Zeta potential values for colloidal suspensions of magnetic nanoparticles (bare and coated)

Material	Zeta potential / mV	Increase of zeta potential / %
Fe_3O_4	−31.9 ± 3.9	–
TA-Fe_3O_4	−39.4 ± 1.1	23.6
Fe_3O_4-TA	−33.4 ± 2.3	5.9

precipitate in dispersion when the TA was present. Figure S2 of the Supplementary Information shows a simple test of stability of the colloidal dispersions for the bare magnetic nanoparticles and hybrid materials after 15 min of rest. It is possible to observe the bare magnetic nanoparticles precipitate and deposit on the bottom of the flask. However, for hybrid materials, the presence of polyphenol compounds makes the nanoparticles more dispersible in aqueous media (pH 6.7), probably due to the negative charge provided by the TA and its large molecular size, which avoids the aggregation phenomena by contribution of both electrostatic repulsion and physical spacing.[42]

Representative TEM images for bare nanoparticles and hybrid Fe_3O_4 suspensions are shown in Figure 4. As expected, bare nanoparticles showed polydispersity, exhibiting significant variations in their sizes and shapes. It can be seen in Figure 4a that the Fe_3O_4 NPs showed sizes between 10 and 35 nm, with several shapes: triangular, rectangular, pentagonal, hexagonal and spherical. This behavior was already expected due to their large surface areas and magnetic dipoles, which follow the tendency to agglomerate, seeking to decrease their surface energies.[11] Furthermore, the TEM images for the TA-Fe_3O_4 NPs indicate the production of elongated particles with sizes ranging between 20-30 nm (nanoneedles), as well as Fe_3O_4 NPs coated with tannic acid showing sizes between 8 and 30 nm (Figure 4b). This reveals that the strategy to add TA before nanoparticle formation does not prevent the agglomeration phenomenon or the production of the nanoparticles with a wide variety of sizes and shapes, as occurred with bare nanoparticles. However, for the Fe_3O_4-TA system (Figure 4c) it was observed that this hybrid material presents a layout very similar to a core-shell system (as shown in Figure 4d), in which the Fe_3O_4 NPs are wrapped in a TA coat. It is apparent that the addition of TA after the Fe_3O_4 NPs production prevented agglomeration and produced NPs almost spherically, with an average diameter of 8 nm. This behavior can be seen clearly in the TEM images, in which the nanoparticles are involved by TA and are close to one another, but do not agglomerate. The physicochemical properties of the developed hybrid ferromagnetic materials are highly

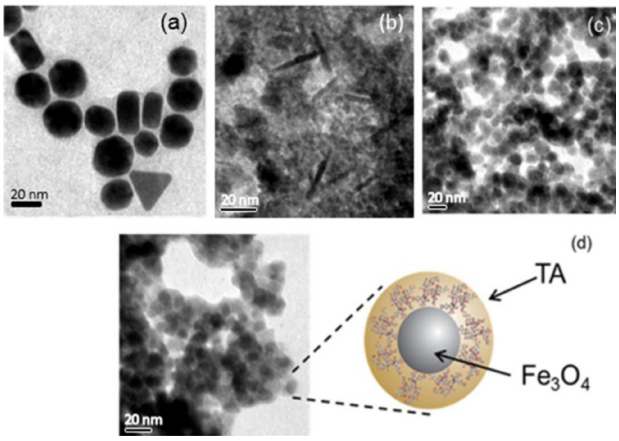

Figure 4. TEM images for (a) bare Fe_3O_4 NPs; (b) TA-Fe_3O_4 NPs; (c) Fe_3O_4-TA NPs and (d) illustration of the core-shell like coverage of TA over Fe_3O_4 nanoparticles in the Fe_3O_4-TA system.

dependent on the preparation conditions, specially the amount of TA compound that is added to the synthesis. These conditions influence the shape of the particles and the amount of TA on its shell. Our results are consistent with Herrera-Becerra *et al.*[21] report that showed the high degree of stabilization and shape control of nanoparticles using related phenolic compounds.

X-ray diffraction was used to investigate the crystalline content of the nanoparticles and hybrid materials. Figure 5 shows the powder XRD patterns of bare and coated Fe_3O_4 (code 082 237 ICSD) nanoparticles with tannic acid and strong Bragg reflection peaks (2θ: 18.3, 30, 35.4, 43.1, 53.4, 57 and 62.5º) assigned to (111), (220), (311), (400), (422), (511), and (440) Miller indices. Crystallographically, magnetite takes on a cubic inverse spinel structure due to the fact that the oxide ions form a face-centered cubic, with the iron(II) and iron(III) cations occupying one-eighth of the tetrahedral and half of the octahedral holes, respectively.[34] These results are in agreement with the works of Yang *et al.*[43] and Zhan *et al.*,[44] who worked with epoxy functionalized Fe_3O_4 and carbon nanotube/Fe_3O_4 systems, respectively. In addition, diffractograms for the Fe_3O_4 and Fe_3O_4-TA illustrate well defined and intense peaks mainly related to the crystallographic plane (311), showing the presence of the crystalline phase of Fe_3O_4 NPs, even after the addition of TA (hybrid materials). The TA potentially interacts through the (111) plane of the Fe_3O_4 NPs. We based this on reports that assert that the (111) phase is the most exposed to the environment and favorable for binding to oxygen atoms.[45] We noticed that the (111) phase does not produce a large XRD peak (Figure 5) due to low intensity typically observed for that plane.

In order to estimate the average size of the crystallite of pure and TA coated Fe_3O_4 NPs, the Scherrer's equation[34]

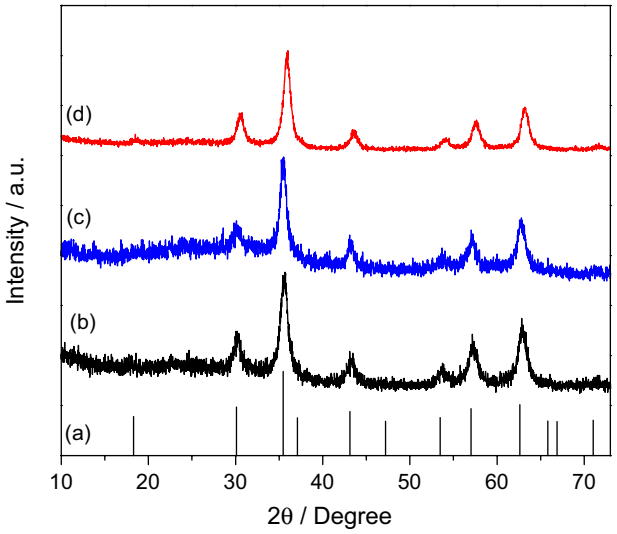

Figure 5. X-Ray diffraction patterns of magnetite: (a) ICSD data; (b) Fe_3O_4; (c) TA-Fe_3O_4; (d) Fe_3O_4-TA.

(equation 3) was applied using the reflection of the cubic inverse spinel structure's $d_{(311)}$ plane.

$$D_{XRD} = (k\lambda / \beta_D \cos\theta) \quad (3)$$

Here, D_{XRD} represents the particle size in nanometers; λ is the wavelength of the radiation (1.54018 Å for Cu-K_α radiation); k is a constant equal to 0.9; β_D is the peak width at half-maximum intensity ((311) peak) and θ is the Bragg angle. It was found that the average sizes of the crystallite are 11.0, 9.0, and 7.0 nm for Fe_3O_4, TA-Fe_3O_4, and Fe_3O_4-TA NPs, respectively. These results showed good agreement with the experimental data obtained by TEM analysis.

We did not observe a reduction in diffraction intensities and shifts of the peaks for TA-Fe_3O_4 and Fe_3O_4-TA systems, because the reduction of peak intensity and shift on diffraction angle are associated to the Fe_3O_4 phase stability/crystallinity and lattice parameters of unit cell, respectively. However, the TA-Fe_3O_4 diffractogram exhibited broader peaks compared to the one obtained from Fe_3O_4-TA, meaning that the interaction between the ions Fe^{II}/Fe^{III} with TA, forming a coordination complex (according to equations 1 and 2), interferes on the way the crystal grows, and so on the final crystallinity and crystal size of the material.

Combining the TEM and XRD findings, we can infer that the TA matrix influenced the supramolecular organization of the Fe_3O_4 NPs crystallites, which led to different crystalline growth depending on the choice of precipitation step, suggesting that the bottom up nanobuilding process depends directly on the supramolecular interactions between the precursors building blocks.[36]

Conclusions

Ferromagnetic hybrid materials prepared through co-precipitation were successfully coated by TA, as evidenced by TEM analysis and FTIR spectra. We could notice that different nanoparticles are obtained depending on the step TA is added to the system, mostly because of the interaction between phases during the crystal growth and ripening. When TA was added after Fe_3O_4 NPs production, particles presented a spherical core-shell-like shape and average diameter of 15 nm. This organization is completely different from that observed for the bare Fe_3O_4 and TA-Fe_3O_4 NPs, suggesting that TA plays a fundamental role in the nucleation and organization of Fe_3O_4 NPs. Based on information from DFT and FTIR analysis, we propose that Fe_3O_4 interacts mainly through carbonyl groups; however, phenolic hydroxyls and aromatic rings also show minor contributions to the NPs stabilization. Since these particles presented better water dispersibility in aqueous media and considering the TA biocompatibility, these hybrid materials may have potential biomedical applications, such as drug-delivery in organism. Finally, our work brings a supramolecular approach that opens up a new alternative to develop hybrid materials with controlled properties and explore their reactivity according to specific chemical reactions (e.g., cancer drugs with organic interfaces).

Supplementary Information

Supplementary data (magnetic activity on dispersion, colloidal stability, and whole optimized structures) are available on supplementary information at http://jbcs.sbq.org.br as PDF file.

Acknowledgements

The authors acknowledge the financial support from CNPq (470996/2011-0 and 304684/2011-2 projects), CAPES (nBioNet), FAPEPI, MICINN (Spain) for project MAT 2011-25870, and CENAPAD-UFC by availability of computational resources used in the development of theoretical calculations.

References

1. Stupp, S. I.; Palmer, L. C.; *Chem. Mat.* **2013**, *26,* 507.
2. Rurack, K.; Martínez-Máñez, R.; *The Supramolecular Chemistry of Organic-Inorganic Hybrid Materials*; John Wiley & Sons: New York, 2010.
3. Silva, A. T. B.; Coelho, A. G.; Lopes, L. C. S.; Martins, M. V. A.;

Crespilho, F. N.; Merkoçi, A.; Silva, W. C.; *J. Braz. Chem. Soc.* **2013,** *24*, 1237.

4. Luz, R. A. S.; Martins, M. V. A.; Magalhães, J. L.; Siqueira, J. R.; Zucolotto, V.; Oliveira, O. N.; Crespilho, F. N.; Silva, W. C.; *Mat. Chem. Phys.* **2011,** *130*, 1072.
5. Wei, P.; Yan, X.; Huang, F.; *Chem. Soc. Rev.* **2015**, *44*, 815.
6. Behrens, S.; *Nanoscale* **2011**, *3*, 877.
7. Zhu, H.; Tao, J.; Wang, W.; Zhou, Y.; Li, P.; Li, Z.; Yan, K.; Wu, S.; Yeung, K. W. K.; Xu, Z.; Xu, H.; Chu, P. K.; *Biomaterials* **2013,** *34,* 2296.
8. Sophie, L.; Silvio, D.; Urs, O. H.; Morteza, M.; *Adv. Colloid. Interf.* **2011,** *166,* 8.
9. Zhou, L.; Yuan, J.; Wei, Y.; *J. Mat. Chem.* **2011**, *21,* 2823.
10. Leslie-Pelecky, D. L.; Rieke, R. D.; *Chem. Mat.* **1996,** *8,* 1770.
11. Xing, Z. H.; Wang, S. S.; Xu, A. W.; *CrystEngComm*. **2014**, *16,* 1482.
12. Peddis, D.; Cannas, C.; Musinu, A.; Ardu, A.; Orrù, F.; Fiorani, D.; Laureti, S.; Rinaldi, D.; Muscas, G.; Concas, G.; Piccaluga, G.; *Chem. Mater.* **2013**, *25,* 2005.
13. Liu, J.; Qiao, S. Z.; Hu, Q. H.; Lu, G. Q.; *Small* **2011,** *7,* 425.
14. Lopes, G. K. B.; Schulman, H. M.; Hermes-Lima, M.; *Biochim. Biophys. Acta, Gen. Subj.* **1999,** *1472,* 142.
15. Wang, Y.; Xu, F.; Zhang, L.; Wei, X.; *J. Nanopart. Res.* **2012**, *15,* 1.
16. Wu, M.; Xiong, Y.; Jia, Y.; Niu, H.; Qi, H.; Ye, J.; Chen, Q.; *Chem. Phys. Let.* **2005**, *401*, 374.
17. Wu, S.; Sun, A.; Zhai, F.; Wang, J.; Xu, X.; Zhang, Q.; Volinsky, A. A.; *Mat. Lett.* **2011**, *65,* 1882.
18. Ai, Z.; Deng, K.; Wan, Q.; Zhang, L.; Lee, S.; *J. Phys. Chem. C* **2010,** *114,* 6237.
19. Prozorov, T.; Mallapragada, S. K.; Narasimhan, B.; Wang, L.; Palo, P.; Nilsen-Hamilton, M.; Williams, T. J.; Bazylinski, D. A.; Prozorov, R.; Canfield, P. C.; *Adv. Funct. Mater.* **2007,** *17,* 951.
20. Herrera-Becerra, R.; Zorrilla, C.; Ascencio, J. A.; *J. Phys. Chem. C* **2007,** *111,* 16147.
21. Herrera-Becerra, R.; Rius, J. L.; Zorrilla, C.; *Apply. Phys. A* **2010,** *100,* 453.
22. Omoike, A. In *Nanoparticles: Synthesis, Stabilization, Passivation, and Functionalization*; Nagarajan, R.; Hatton, T. A., eds; American Chemical Society: Washington, 2008, ch. 8.
23. Kohn, W.; Sham, L. J.; *Phys. Rev.* **1965,** *140,* 1133.
24. Becke, A. D.; *J. Chem. Phys.* **1993**, *98,* 5648.
25. Lee, C.; Yang, W.; Parr, R. G.; *Phys. Rev. B* **1988,** *37,* 785.
26. Hariharan, P. C.; Pople, J. A.; *Theoret. Chim. Acta* **1973,** *28,* 213.
27. Hay, P. J.; Wadt, W. R.; *J. Chem. Phys.* **1985***, 82*, 270.
28. Hay, P. J.; Wadt, W. R.; *J. Chem. Phys.* **1985,** *82,* 299.
29. Wadt, W. R.; Hay, P. J.; *J. Chem. Phys.* **1985,** *82,* 284.
30. Frisch, M. J.; Trucks, G. W.; Schlegel, H. B.; Scuseria, G. E.; Robb, M. A.; Cheeseman, J. R.; Scalmani, G.; Barone, V.; Mennucci, B.; Petersson, G. A.; Nakatsuji, H.; Caricato, M.; Li, X.; Hratchian, H. P.; Izmaylov, A. F.; Bloino, J.; Zheng, G.; Sonnenberg, J. L.; Hada, M.; Ehara, M.; Toyota, K.; Fukuda, R.; Hasegawa, J.; Ishida, M.; Nakajima, T.; Honda, Y.; Kitao, O.; Nakai, H.; Vreven, T.; Montgomery, J. J. A.; Peralta, J. E.; Ogliaro, F.; Bearpark, M.; Heyd, J. J.; Brothers, E.; Kudin, K. N.; Staroverov, V. N.; Kobayashi, R.; Normand, J.; Raghavachari, K.; Rendell, A.; Burant, J. C.; Iyengar, S. S.; Tomasi, J.; Cossi, M.; Rega, N.; Millam, J. M.; Klene, M.; Knox, J. E.; Cross, J. B.; Bakken, V.; Adamo, C.; Jaramillo, J.; Gomperts, R.; Stratmann, R. E.; Yazyev, O.; Austin, A. J.; Cammi, R.; Pomelli, C.; Ochterski, J. W.; Martin, R. L.; Morokuma, K.; Zakrzewski, V. G.; Voth, G. A.; Salvador, P.; Dannenberg, J. J.; Dapprich, S.; Daniels, A. D.; Farkas, Ö.; Foresman, J. B.; Ortiz, J. V.; Cioslowski, J.; Fox, D. J.; *Gaussian 09*, *Revision D.01*; Gaussian, Inc., England, 2009.
31. Huang, D. M.; Cao, D. B.; Li, Y. W.; Jiao, H.; *J. Phys. Chem. B* **2006,** *110,* 13920.
32. Lei, Y.; Tang, Z.; Liao, R.; Guo, B.; *Green Chem.* **2011,** *13,* 1655.
33. Perron, N.; Brumaghim, J.; *Cell Biochem. Biophys.* **2009,** *53*, 75.
34. Marangoni, V.; Martins, M. V. A.; Souza, J.; Oliveira, O. N.; Zucolotto, V.; Crespilho, F. N.; *J. Nanopart. Res.* **2012**, *14*, 1.
35. Pereira, A. R.; Iost, R. M.; Martins, M. V. A.; Yokomizo, C. H.; Silva, W. C.; Nantes, I. L.; Crespilho, F. N.; *Phys. Chem. Chem. Phys.* **2011**, *13*, 12155.
36. Martins, M. V. A.; Bonfim, C.; Silva, W. C.; Crespilho, F. N.; *Electrochem. Commun.* **2010**, *12,* 1509.
37. Jaén, J. A.; Araúz, E. Y.; Iglesias, J.; Delgado, Y.; *Hyperfine Interact.* **2003,** *148,* 199.
38. Iglesias, J.; García de Saldaña, E.; Jaén, J. A.; *Hyperfine Interact.* **2001,** *134,* 109.
39. Zhao, G.; Feng, J. J.; Zhang, Q. L.; Li, S. P.; Chen, H. Y.; *Chem. Mater.* **2005,** *17,* 3154.
40. Maharramov, A. M.; Alieva, I. N.; Abbasova, G. D.; Ramazanov, M. A.; Nabiyev, N. S.; Saboktakin, M. R.; *Dig. J. Nanomater. Bios*. **2011,** *6,* 419.
41. Yang, C.; Du, J.; Peng, Q.; Qiao, R.; Chen, W.; Xu, C.; Shuai, Z.; Gao, M.; *J. Phys. Chem. B* **2009**, *113,* 5052.
42. Mallick, K.; Witcomb, M. J.; Scurrell, M. S.; *J. Mater. Sci.* **2004,** *39,* 4459.
43. Yang, L.; Gao, Z.; Guo, Y.; Zhan, W.; Guo, Y.; Wang, Y.; Lu, G.; *Microporous Mesoporous Mater.* **2014,** *190,* 17.
44. Zhan, Y.; Zhao, R.; Lei, Y.; Meng, F.; Zhong, J.; Liu, X.; *J. Magn. Magn. Mater.* **2011,** *323,* 1006.
45. Santos-Carballal, D.; Roldan, A.; Grau-Crespo, R.; de Leeuw, N. H.; *Phys. Chem. Chem. Phys.* **2014,** *16,* 21082.

Submitted: March 12, 2015
Published online: November 24, 2015